T2R2 東京工業大学リサーチリポジトリ
Tokyo Tech Research Repository

論文 / 著書情報
Article / Book Information

Title	Performance recovery of a repaired 4-storey reinforced concrete structure subjected to shake-table testing
Authors	Alex Shegay, Kota Miura, Akira Mikawa, Masaki Maeda, Matsutaro Seki
Citation	Earthquake Engineering & Structural Dynamics, Volume 52, Issue 5, pp. 1339-1359
Pub. date	2023, 1
DOI	https://doi.org/10.1002/eqe.3818
Creative Commons	Information is in the article.

Powered by T2R2 (Tokyo Institute Research Repository)

Check for updates

Received: 2 July 2022 | Revised: 21 December 2022 | Accepted: 29 December 2022

DOI: 10.1002/eqe.3818

RESEARCH ARTICLE

WILEY

Performance recovery of a repaired 4-storey reinforced concrete structure subjected to shake-table testing

Alex V. Shegay[1] | **Kota Miura**[2] | **Mikawa Akira**[3] | **Masaki Maeda**[3] | **Matsutaro Seki**[4]

[1]FIRST, Tokyo Institute of Technology, Yokohama, Japan

[2]Obayashi Corporation, Kiyose, Japan

[3]Department of Architecture and Building Science, Tohoku University, Sendai, Japan

[4]Building Research Institute, Tsukuba, Japan

Correspondence
Alex V. Shegay, FIRST, Tokyo Institute of Technology, Yokohama, Japan.
Email: shegay.a.aa@m.titech.ac.jp

Funding information
Japan Science and Technology Agency, Grant/Award Number: JPMJOP1723; Obayashi Corporation

Abstract

Understanding the effects of repair on reinforced concrete (RC) structures is critical to evaluating their performance in future earthquakes. In this research, a system-level approach is taken by repairing a previously damaged ¼ scale 4-storey RC structure and subjecting it to a series of dynamic excitations via shake table testing. The repair was undertaken using common construction materials with the primary motivation of restoring original performance. The performance of the repaired structure was compared to that of the original structure prior to repairs. It was found that overall initial stiffness of the structure was recovered to 66% of the original initial stiffness and was generally higher in floors where more intensive repair works were undertaken. Damping capacity was quantified via equivalent viscous damping ratio using three different methods. Regardless of the calculation method, the damping capacity recovery was around 80% for low-moderate drifts and 100% for high drifts. While collapse was not induced in the structure, drift ratio demands of over 5% could be achieved both before and after repairs, suggesting a full practical recovery of deformation capacity. Structural strength of the repaired structure was found to be 17% higher than that of the original structure.

KEYWORDS

epoxy injection, equivalent viscous damping, performance recovery, reinforced concrete, repair, shake-table, strain aging

1 | INTRODUCTION

Reinforced concrete (RC) structures damaged in earthquakes will typically be subjected to one of two decisions: structural repair or demolition (followed by rebuilding if necessary). While the latter will ensure a damage-free structure, this is often not the most economical decision, nor is it reflective of the disaster resilience and infrastructure sustainability goals targeted within United Nation's 17 Sustainability Development Goals.[1] Despite this, RC buildings have seen high demolition rates in previous earthquakes, even in cases where relatively low levels of damage were sustained.[2] While social factors

This is an open access article under the terms of the Creative Commons Attribution License, which permits use, distribution and reproduction in any medium, provided the original work is properly cited.
© 2023 The Authors. *Earthquake Engineering & Structural Dynamics* published by John Wiley & Sons Ltd.

10969845, 0, Downloaded from https://onlinelibrary.wiley.com/doi/10.1002/eqe.3818 by Tokyo Institute Of Technology, Wiley Online Library on [16/01/2023]. See the Terms and Conditions (https://onlinelibrary.wiley.com/terms-and-conditions) on Wiley Online Library for rules of use; OA articles are governed by the applicable Creative Commons License

NOVELTY

- Global performance recovery of a 4-storey reinforced concrete structure repaired using traditional techniques investigated via shake table testing.
- Less visual damage observed following repair due to repair materials being less stiff than the original materials.
- Natural period measurements following each repair stage showed that epoxy injection of beams and slabs resulted in the highest recovery of initial structural stiffness.
- Initial stiffness recovery of 66% was achieved using extensive epoxy injection.
- Full recovery of deformation capacity and damping capacity achieved.
- Reinforcement strain aging was shown to cause an increase in strength of 17% after repair of the original structure.

and insurance are almost always at play, limited available guidance on suitable structural repair techniques and an overall lack of confidence in the future performance of the repaired structure are key contributing factors to the high demolition rates.

Seismic performance recovery achieved through repair for any specific performance characteristics can be expressed by a performance recovery factor, λ. As shown in Equation (1), λ can be defined as a quotient of some performance characteristic of a repaired structure, ${}_rQ$, to the same performance characteristic in an undamaged structure, ${}_uQ$.

$$\lambda = \frac{{}_rQ}{{}_uQ} \tag{1}$$

Subscripts can be suffixed to the terms in Equation (1) to identify the performance characteristic. In this study, subscripts of "*K*," "*d*," "*dc*" and "*s*" will be used to represent "stiffness," "damping capacity," "deformation capacity" and "strength," respectively. One existing document providing guidance on the expected structural performance recovery factors of repaired members is the Federal Emergency Management Agency's "Evaluation of Earthquake Damaged Concrete and Masonry Wall Buildings" manual (hereinafter "FEMA 306").[3] In FEMA 306 the performance recovery factors for strength, effective yield stiffness and deformation capacity are provided for several RC and masonry components that are repaired in accordance with available guidelines.[4] These recovery factors are intended to be used to adjust simplified member backbone models defined in the "NEHRP Guidelines for the Seismic Rehabilitation of Buildings"[5] (superseded by "ASCE Seismic Evaluation and Retrofit of Existing Buildings"[6]) when performing numerical analysis of repaired structures. As FEMA 306 specifically targets response of wall buildings, performance recovery factors for moment frame members (beams and columns) are not included. A lesser-known guideline for performance recovery factors of repaired RC structures is the Japan Building Disaster Prevention Association's "Guidelines for Damage Classification Criteria and Restoration Techniques of Damaged Buildings" (hereinafter "JBDPA Guidelines").[7] In this document, performance recovery factors for several repaired member types (beams, columns, and walls) are provided corresponding to various levels of damage severity and several repair strategies (crack epoxy injection, concrete replacement, or strengthening). These performance recovery factors are given as a range; however, unlike FEMA 306 there is no distinction between which structural performance characteristic (i.e., strength, stiffness, deformation capacity) will recover to what degree. The ambiguity makes these factors difficult to implement with confidence in analysis of repaired structures. A summary of the performance recovery factors listed in the JBDPA Guidelines is provided in Appendix A.

In addition to the above guidelines, member-level repair studies have been conducted on RC beams,[8–11] columns,[12] beam-column joints,[13] and walls.[14–16] Though there are differences in the level of initial damage and the extent of repair implemented among these studies, it can be generalized that strength is recovered to at least 100% (with one exception[16]); energy dissipation (calculated from hysteretic loop area) is recovered to 95%–100%; secant stiffness to yield by 40%–75% and deformation capacity to 100% (exception of[16]). As these studies cover a broad range of parameters, it is not immediately clear how these levels of recovery will manifest in the overall system-level performance of repaired RC structures. With exception of,[17] which will be referred to in subsequent discussions, research on system-level performance recovery of repaired structures is highly limited. In this paper, the effectiveness of repair on the system-level structural performance recovery is investigated by shake-table testing of a previously damaged ¼-scale 4-storey RC structure that exhibited flexural damage characteristics (flexural cracks, spalling of concrete, buckling of reinforcement).[18] As performance is thought to

10969845, 0, Downloaded from https://onlinelibrary.wiley.com/doi/10.1002/eqe.3818 by Tokyo Institute Of Technology, Wiley Online Library on [16/01/2023]. See the Terms and Conditions (https://onlinelibrary.wiley.com/terms-and-conditions) on Wiley Online Library for rules of use; OA articles are governed by the applicable Creative Commons License

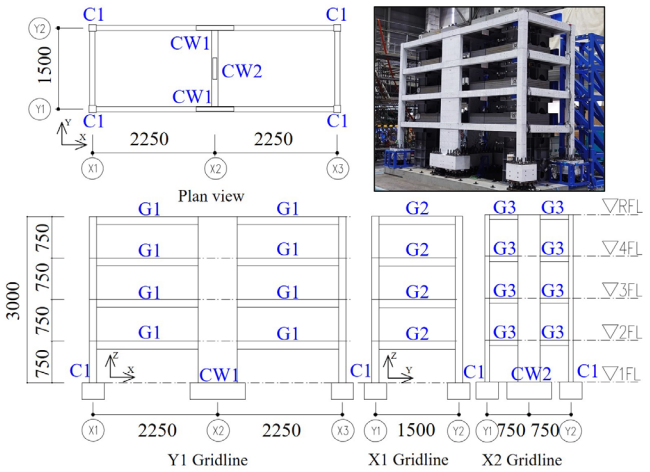

FIGURE 1 Dimensions of Original structure (units: mm)

TABLE 1 Details of member sections comprising the test structure (units: mm)

Member	Column	Wall		Beam			
Name	C1	CW1	CW2	G1	G2	G3	Slab
Section		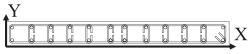	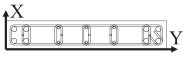				
Size (mm)	130 × 130	80 × 700	70 × 400	100 × 140	100 × 150	120 × 90	70 (thick)
Main bar	6-D10	24-D10	8-D13 + 6-D6	6-D6	8-D6	4-D6	D4@80 (X-dir.)
Hoop/stirrup	D4@60	D4@60	D4@100 (cross-ties D4@50)	D4@60	D4@60	D6@30	D4@60 (Y-dir.)

depend on the level of initial damage, the research presented herein takes a "limiting-case" approach by considering the effect of repairs on a severely damaged structure. Repair is defined in this paper as work that targets restoration of original performance and is distinct from "strengthening," which targets an enhancement of performance relative to the original structure.

2 | RESEARCH OBJECTIVE

The objective of this paper is to investigate the degree of system-level performance recovery achieved in RC structures exhibiting flexural damage characteristics, by use of relatively basic structural repair techniques and common repair materials. The structural performance characteristics considered are structural stiffness, damping capacity, deformation capacity, and strength.

3 | ORIGINAL STRUCTURE EXPERIMENTAL PROGRAM OVERVIEW

In this study, a ¼-scale 4-storey RC frame-wall structure tested in a previous study (hereinafter referred to as the "Original" structure)[18] was repaired and re-tested on a shake-table (hereinafter referred to as the "Repaired" structure). The details of the Original test structure and its seismic performance are revisited briefly in this section (details can be found in a previous publication[18]). The test structure's overall dimensions are shown in Figure 1 and details of the member cross-sections of the structure (denoted CW1/CW2 for walls, C1 for columns, and G1/G2/G3 for beams) are shown in Table 1. The Original structure was designed as a new office building located in Tokyo on Type 2 soil,[19] using current Japanese seismic design[20] and RC standards.[21] The design methodology followed principles to achieve a weak-beam strong-column inelastic mechanism – a common approach in modern seismic design of buildings around the world (e.g.,[22–24]). Thus, flexural hinges were designed to develop in the beam ends, and base of columns and

10969845, 0, Downloaded from https://onlinelibrary.wiley.com/doi/10.1002/eqe.3818 by Tokyo Institute Of Technology, Wiley Online Library on [16/01/2023]. See the Terms and Conditions (https://onlinelibrary.wiley.com/terms-and-conditions) on Wiley Online Library for rules of use; OA articles are governed by the applicable Creative Commons License

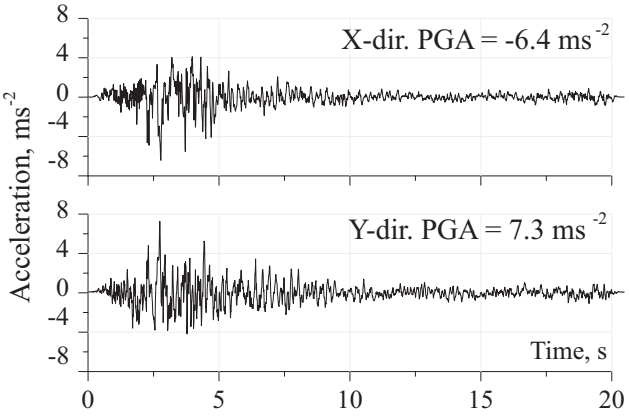

FIGURE 2 Artificial acceleration time history records used in the X- and Y-directions of the test structure

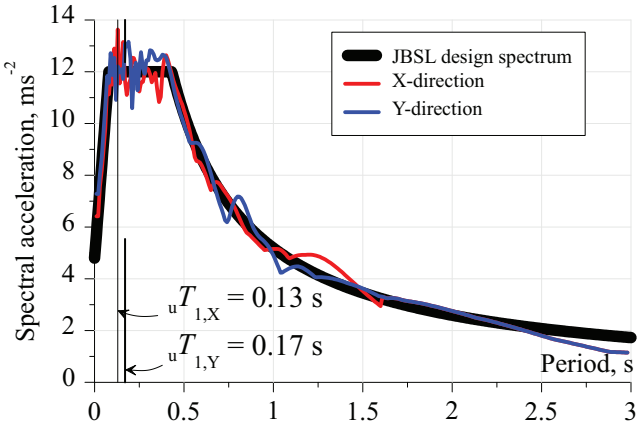

FIGURE 3 Acceleration design spectrum per[19] plotted with the acceleration response spectrum of the artificial records used in the experiments

walls. All longitudinal and transverse reinforcement used in the structure was of deformed type. It is noted that due to reinforcement diameter scaling constraints, the transverse reinforcement spacing in the columns (60 mm) exceeded that required by the code (accounting for scale, 50 mm). As part of the objectives of the original study, the structure was designed such that the in-plane walls would carry ~60% and ~30% of the total base shear in the X- and Y-directions, respectively.

3.1 | Ground motion characteristics

In both the Original and Repaired structure experiments, the same artificial ground motion pair shown in Figure 2 was used. The time of the ground motion was scaled by half to account for the ¼ scale of the structure. The phase of the ground motion pair was the 1995 Kobe earthquake recorded in the North-South (used in the test structure X-direction shaking) and East-West (used in the test structure Y-direction shaking) directions at the "JMA Kobe" site. The ground motion pair was modified to match the Level 2 "extremely rare" earthquake design spectrum for Type 2 soils in Tokyo, based on specifications in the Japanese Building Standard Law (JBSL).[19] As can be seen in Figure 3, a close match was achieved between the ground motion acceleration response spectra and the design acceleration spectrum. The loading sequence in both experimental programs, shown in Table 5, consisted of uniformly scaling the earthquake acceleration demand over a series of nine excitations (hereinafter referred to as "Runs"). The first mode period of the Original structure prior to testing was determined via white noise tests to be ${}_uT_{1,X} = 0.13$ s and ${}_uT_{1,Y} = 0.17$ s in the X- and Y-directions, respectively.

10969845, 0, Downloaded from https://onlinelibrary.wiley.com/doi/10.1002/eqe.3818 by Tokyo Institute Of Technology, Wiley Online Library on [16/01/2023]. See the Terms and Conditions (https://onlinelibrary.wiley.com/terms-and-conditions) on Wiley Online Library for rules of use; OA articles are governed by the applicable Creative Commons License

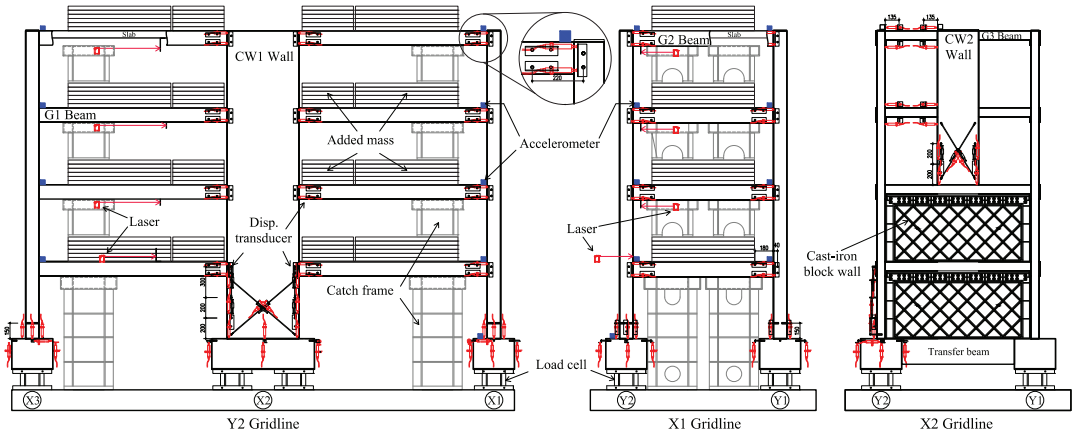

FIGURE 4 Key instrumentation used in the Repaired structure (nominally identical in the Original structure)

3.2 | Instrumentation

A layout of the main instrumentation used in the Repaired structure (nominally identical to that used in the Original structure) is shown in Figure 4. Laser transducers were placed on each story to measure the inter-story displacements. The first-floor laser displacement measurements were taken from an external reference point on the shake-table. Displacement transducers were placed at the hinge locations of selected beams, columns, and walls to measure plastic hinge rotations. Tri-axial load cells (calibrated uni-axially) were placed under each foundation. Accelerometers were placed on each floor at each corner of the structure (immediately beside columns). Accelerometers were also placed at the foundation level to measure the real input acceleration demands. During construction, strain gauges were attached to longitudinal reinforcement in the plastic hinges of several selected members.

3.3 | Results of testing of the Original structure

In this section, a brief explanation of the loading sequence and damage progression of the Original structure is provided. For details, the reader is referred to.[18] Examples of final damage observed at the end of the testing (and after correction of residual drift) is shown in Figure 6. Cracking throughout the structure was observed following Run 1. Longitudinal reinforcement in the CW1 walls was determined to yield at Run 3, followed by yielding in all measured beam and column hinges by the end of Run 4. During Run 5, extensive spalling of end region cover concrete was observed in the CW1 walls, while the CW2 wall experienced a diagonal shear failure in the first two floors. With subsequent runs, inter-story drift gradually increased, as did the extent of spalling in all member types. During Run 9, the CW1 walls experienced flexural failure, characterized by crushing of the core concrete in the end regions and buckling of the first two rows of longitudinal reinforcement, as shown in Figure 6D. Damage of the X3-gridline columns (subjected to high compression stresses during the main pulse of the excitation) was characterized by spalling of the concrete in the plastic hinge region as shown in Figure 6C. Slight curvature was observed in the longitudinal reinforcement of the X3-Y1 column, suggesting incipient buckling. The X1-gridline columns had slight spalling near the foundation interface; however, no reinforcement was exposed (Figure 6B). All beams experienced rotations in the range of 0.02–0.05 radians as measured by displacement transducers in the plastic hinge zones. Several beam hinges forming into the wall experienced concrete spalling (Figure 8B). At the conclusion of the experiment, maximum residual inter-story drift ratios of 2.10% and 1.33% were recorded in the X- and Y-directions, respectively.

4 | REPAIR OF THE ORIGINAL STRUCTURE

The repair objective in the X-direction was to reinstate the original seismic performance using commonly available materials and relatively straightforward repair methodologies. In the Y-direction, in addition to the basic repairs used in the X-direction, strengthening of the structure was also performed using proprietary methods as part of a separate study.[25]

10969845, 0, Downloaded from https://onlinelibrary.wiley.com/doi/10.1002/eqe.3818 by Tokyo Institute Of Technology, Wiley Online Library on [16/01/2023]. See the Terms and Conditions (https://onlinelibrary.wiley.com/terms-and-conditions) on Wiley Online Library for rules of use; OA articles are governed by the applicable Creative Commons License

TABLE 2 Description of repair works, and materials used for each repair class

Repair Class	[Damage level][a] damage	Repair technique	Material
1	[I]: Visible cracks but no spalling of concrete	• Epoxy injection of cracks >0.05 mm in width[b]	Dyflex EverBond EP-400 epoxy resin
2a	[II–III]: Spalling of cover concrete not revealing reinforcement	• Repair Class 1 • Patching with polymer cement	Refremol Set polymer cement
2b	[III–IV]: Spalling of cover concrete revealing reinforcement	• Repair Class 1 • Patching with epoxy mortar	Sikadur-41 epoxy mortar
3	[V]: Severe buckling of longitudinal reinforcement, core concrete crushing	• Repair Class 1 • Removal of damaged concrete • Cutting of buckled bars • Splice welding of new bars • Recasting removed concrete	50 MPa concrete SD345 reinforcement
4	[V]: Shear failure of concrete wall	• Removal of wall and welding anchor plate to cut bars • Fixing of perimeter steel frame to concrete face via epoxy resin • Installation of cast-iron block wall	Cast-iron block wall Sikadur 30 epoxy resin

[a]Damage level is as defined in the JBDPA Guidelines[7].
[b]Based on in-situ (i.e., unscaled) crack width measurement.

The scope of this paper is to investigate the effect of basic repair techniques; thus, further discussions on repair and performance recovery is focused mainly on the X-direction of the Repaired structure. For completion, some brief explanation of the Y-direction repair work is also provided in this section.

4.1 | Repair policy

Prior to undertaking the repair work, the structure's residual deformation was corrected in both directions. This was achieved by statically applying external lateral forces to the 2nd and 4th stories of the structure until the residual inter-story drift reduced to below 0.2% (based on an average of five measurement locations per floor) once the external loads were released. It is acknowledged that correction of residual deformation is generally impractical in real-life application; however, to meet the study's objective of evaluating the effects of basic repair techniques, a fair comparison to the Original structure was given priority. Therefore, it was decided to reduce other major influencing factors (i.e., p-delta effects) that would hinder this comparison. Following correction of residual deformation, the structure was moved off the shake-table test to conduct the repairs (full vertical and foundation lateral bracing was provided to the structure to prevent further damage during relocation). The repair work in the X-direction did not include any changes in cross-section dimensions, steel reinforcement ratios, or any repair techniques that could otherwise be considered to enhance performance relative to the Original structure. The repair works undertaken were divided into five classes, and the class adopted for each structural member was decided based on the member damage level. Damage level definitions were adopted from the JBDPA Guidelines,[7,26] and are summarized in Appendix B. The repair class definitions and the corresponding repair materials used are described in Table 2. The repair methodology within each class was based on a combination of guidance provided in the JBDPA Guidelines,[7] the Japan Building Conservation Center's Building Repair Works Guidelines,[27] and discussions of "best-practice" with the contractor employed to carry out the repair. The repair class assigned to each member throughout the structure is shown in Figure 5.

Typical before and after photos for each repair class are shown in Figure 6. For Repair Class 1, all cracks exceeding an in-situ width measurement of 0.05 mm found in beams, columns and walls were epoxy injected by a hand-operated applicator gun. The 0.05 mm width limit was targeted to account for the structure's reduced scale, given the typical injection limit capability in practice is around 0.2 mm. This lower limit was advised possible by the contractor based on the low viscosity properties of the chosen epoxy resin. For cracks in the floor slabs, it was deemed impractical and unrealistic to inject all the cracks due to the large surface area; instead, only the cracks in the slab that propagated to the beams, columns, or walls were injected (i.e., cracks originating *and* terminating internally in the slab were not injected). Slab

10969845, 0, Downloaded from https://onlinelibrary.wiley.com/doi/10.1002/eqe.3818 by Tokyo Institute Of Technology, Wiley Online Library on [16/01/2023]. See the Terms and Conditions (https://onlinelibrary.wiley.com/terms-and-conditions) on Wiley Online Library for rules of use; OA articles are governed by the applicable Creative Commons License

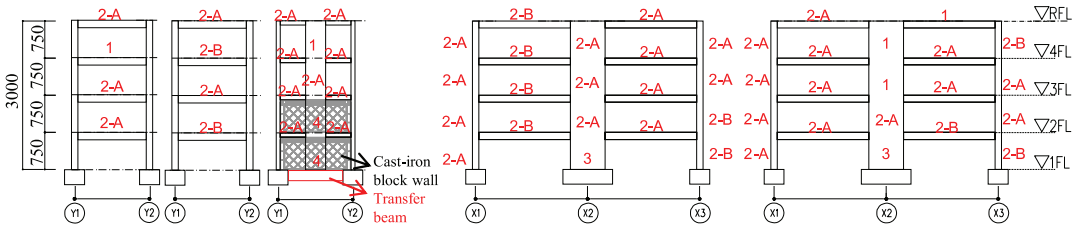

(A) X1, X3 and X2 gridlines (B) Y1 and Y2 gridlines

FIGURE 5 Repair classification of each member of the structure

(A) Class 1: Slab epoxy crack injection (B) Class 2a: polymer cement mortar patching (C) Class 2b epoxy mortar patching

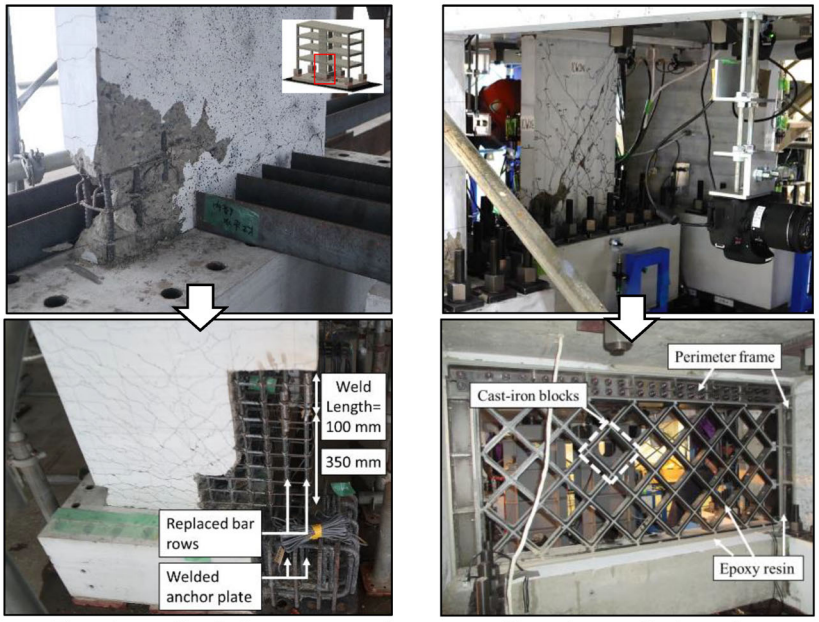

(E) Class 3: Wall reinforcement and concrete replacement (E) Class 4: Installation of cast-iron block wall

FIGURE 6 Typical examples for each repair class listed in Table 2

10969845, 0, Downloaded from https://onlinelibrary.wiley.com/doi/10.1002/eqe.3818 by Tokyo Institute Of Technology, Wiley Online Library on [16/01/2023]. See the Terms and Conditions (https://onlinelibrary.wiley.com/terms-and-conditions) on Wiley Online Library for rules of use; OA articles are governed by the applicable Creative Commons License

TABLE 3 Tested characteristics of the original construction and repair materials (concrete, mortar and epoxy resin)

	Test date	Ultimate compressive stress, MPa	Microstrain at peak stress	Young's modulus, MPa
Original				
30 MPa concrete	Dec 2019	53.1	2700	2.97×10^4
Repair				
30 MPa concrete	Dec 2020	51.1	3160	2.67×10^4
Epoxy mortar	Dec 2020	53.9	39000	0.55×10^4
Polymer cement mortar[a]	-	59.9	-	-
	Viscosity MPa/s	Tensile strength, MPa		
Epoxy resin[a]	130	47.9		

[a]Specified properties listed as no material test was conducted.

cracks that did not meet these criteria were deemed to not be from flexural damage, but the result of stresses developing from the anchoring of the additional floor masses. For Repair Class 2a, polymer cement mortar was used where spalling was not severe enough to expose any reinforcement. In areas of spalling where longitudinal reinforcement was exposed (Figure 6C), epoxy mortar was used for patching (Repair Class 2b) because better adhesion could be achieved to the original material compared to using polymer cement. This approach is also in accordance with guidance in.[27] For Repair Class 3, concrete was removed such that buckled longitudinal reinforcement could be extracted and replacement reinforcement could be lap-splice welded outside the plastic hinge zone (assumed as half the wall length). The length of the weld was ten times the bar diameter on both sides of the splice as recommended in.[7] Welds in the first and second row of reinforcement were staggered by half the weld length as shown in Figure 6D. The bottom of the reinforcement was anchored into the foundation by welding a steel plate to the bottom end of the bar. The repaired area was recast using a concrete mix with similar strength characteristics to the original material. Repair Class 4 was only applied to the area where the CW2 wall had undergone a shear failure in the Y-direction, as shown in Figure 6E. The damaged CW2 wall was completely removed from the 1st and 2nd floors, and a proprietary cast-iron block wall[28] was installed in its place (Figure 6E). The cast-iron blocks ($122 \times 122 \times 40$(depth) $\times$ 8(thick) mm hollow square sections) were stacked diagonally and adhered to each other with epoxy resin. The cast-iron blocks were installed within a perimeter steel frame, which required a continuous concrete support along the base. The bottom support was provided by replacing the original foundation underneath the CW2 with a transfer beam spanning between the foundations of the CW1 walls. The perimeter steel frame was fixed to the surrounding concrete by a 6 mm layer of epoxy resin. Given the weak tensile adhesion of the base of the cast-iron block wall to the transfer beam below it (2.5 MPa over an 80 mm width), the wall was not expected to have significant strength in its out-of-plane response and therefore a negligible contribution to the X-direction response. Under this assumption (confirmed in a later section), the Repair structure X-direction response could be studied in isolation of the strengthening effects of the Y-direction. It is also noted that the net increase in story mass from the installation of the cast-iron block wall was around 1% compared to the Original structure, which was considered to be negligible. The performance of the structure in the Y-direction is outside the scope of this paper, instead, the reader is referred to another publication.[25]

4.2 | Material properties

Original construction and repair material characteristics are in summarized in Tables 3 and 4 for cementitious/epoxy and steel materials, respectively. Repair materials were selected to achieve a close match of physical characteristics to the original materials, unless guided otherwise by the contractor (in order to represent common industry practice in Japan). For example, epoxy mortar has a Young's modulus that is 19% of the original concrete; however, it is preferred for large concrete patching repairs due to its ease of application and superior adhesion properties. Polymer cement mortar (specified 28-day compressive strength of 59.9 MPa) was not tested as only small quantities were used for superficial Class 2a repairs. The strengths of the tested repair materials all matched well with the original construction materials (though the strength of the original concrete may have been higher than the properties listed in Table 3 due to time curing effects).

10969845, 0, Downloaded from https://onlinelibrary.wiley.com/doi/10.1002/eqe.3818 by Tokyo Institute Of Technology, Wiley Online Library on [16/01/2023]. See the Terms and Conditions (https://onlinelibrary.wiley.com/terms-and-conditions) on Wiley Online Library for rules of use; OA articles are governed by the applicable Creative Commons License

TABLE 4 Tested characteristics of the original construction and repair reinforcement materials

Diameter	Test date	Grade	Yield stress, MPa	Ultimate elongation, %	Ultimate stress, MPa	Young's modulus, MPa
Original						
D4	Dec 2019	SD295A	402	-	533	1.90×10^5
D6	Dec 2019	SD345	419	24.1	613	1.97×10^5
D10	Dec 2019	SD345	339	27.9	562	1.93×10^5
D13	Dec 2019	SD390	407	19.2	602	1.95×10^5
Repair						
D4	Dec 2020	SD295A	384	16.1	528	-[a]
D10	Dec 2020	SD345	350	23.7	558	1.95×10^5

[a]Unreliable measurement.

5 | EFFECTS OF EACH STAGE OF REPAIR ON STRUCTURAL STIFFNESS

The natural vibration period of the structure was measured at several stages throughout the repair process to understand the level of stiffness recovery that was achieved after each repair stage. Ambient vibrations of the structure were measured using high-sensitivity accelerometers placed at the X1-Y2 and X3-Y1 corners of the structure, both at the foundation and roof levels (four locations total). The first natural period was estimated by the first peak observed in the transfer function of the roof to foundation acceleration response. As well as an initial natural period measurement taken of the Original undamaged structure (stage "0"), measurements were taken at the following five stages of repair: (1) after relocation of the damaged Original structure to the repair site (structure foundation not fixed) and prior to beginning of repairs; (2) after repair of the CW1 walls and removal of the CW2 walls; (3) after mortar/cement patching and epoxy crack injection of the columns and walls; (4) after mortar/cement patching and epoxy crack injection of beams and slabs; and (5) after re-fixing of the structure to the shake-table. It is noted that the natural period measurement at stage "0" was done with additional weight added to the structure (not present during the repair stages); thus, adjustment of the measured natural period, ${}_uT_{1,X}$, was made using Equation (2) to enable direct comparison to the five repair stages. Use of this equation is appropriate assuming the vibration mode shape of the structure does not change during the repair and the ratio of first mode effective mass is equal to the total mass.

$$T_0 = \sqrt{m/(m+M)} \times {}_uT_{1,X} \tag{2}$$

where m is the self-weight of the structure, M is the additional weight added to satisfy structural similitude, and T_0 is the first natural period of the Original structure without the additional weight.

By assuming the structure to be a single degree of freedom system, the change in natural period following the ith repair stage, T_i, relative to that of the Original undamaged structure, T_0, can be directly related to a corresponding change in structural stiffness (i.e., stiffness recovery factor). using the following equation:

$$\frac{K_i}{K_0} = \left(\frac{T_0}{T_i}\right)^2 \tag{3}$$

where K_0 is the stiffness of the Original undamaged structure and K_i is the stiffness of the Repaired structure following the ith repair stage. The results of Equation (3) for each repair stage are plotted in Figure 7. From Figure 7 it can be observed that repairs to the wall (stage 2) and columns (stage 3) resulted in incremental increases in structural stiffness of 32% and 17% (relative to stage 1), respectively. Repair of the beams and slabs, (stage 4; corresponding to the largest volume of crack epoxy injection), resulted in the largest increase of stiffness relative to stage 1 of 151%. After re-attaching the structure to the shake-table (stage 5), the final Repaired structure's natural period was measured to have recovered to 87% of the Original structure's natural period (i.e., relative to stage 0), suggesting an overall stiffness recovery of 75%. This is considerably higher than the 70% recovery of natural period (50% stiffness recovery) achieved in a full-scale, 7-storey, repaired structure in a previous study.[17] It is thought that the comprehensive epoxy injection repair policy adopted in the

10969845, 0, Downloaded from https://onlinelibrary.wiley.com/doi/10.1002/eqe.3818 by Tokyo Institute Of Technology, Wiley Online Library on [16/01/2023]. See the Terms and Conditions (https://onlinelibrary.wiley.com/terms-and-conditions) on Wiley Online Library for rules of use; OA articles are governed by the applicable Creative Commons License

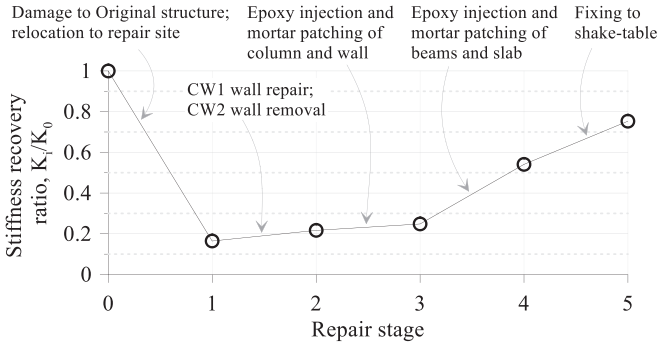

FIGURE 7 Estimated stiffness recovery factor from natural period measurements at each repair stage

present study (compared to[17] where only "major cracks" were injected) is the main reason for the higher stiffness recovery achieved.

6 | RESPONSE OF REPAIRED STRUCTURE

6.1 | Repaired structure loading protocol

The Repaired structure was subjected to a total of ten excitations ("Runs"). The magnitude of the input-ground-motion used for each Run is listed in Table 5. The ground motion magnitude decision policy in the Repaired test was to reproduce the maximum roof drift ratio measured in each Run of the Original structure, to enable convenient performance comparison. An exception was Run 6, where the objective was to reproduce the roof drift of Run 5. The instrumentation plan for the Repaired structure, shown in Figure 4, was nominally identical to that of the Original structure.

6.2 | Damage description

The peak inter-story drift ratio, Δ_{max}, peak base shear, V_{max} and salient damage characteristics following each Run are summarized in Table 5. A photo comparison of the most severely damaged members for the Original structure (after correction of residual drift and prior to initiating repair) and Repaired structure is shown in Figure 8. Base shear of the structure was determined from the sum of the accelerations of each story multiplied by respective floor masses, while inter-story drift ratios were calculated from laser measurements at each floor.

Damage observed up to Run 4 was generally consistent between the Original and Repaired structures. A reduced structural stiffness resulted in slightly lower strengths observed in the Repaired structure for each run until Run 4 compared to the Original structure. At Run 4, the Repaired structure's strength exceeded that of the Original structure. Following this run a crack running along the full base length of the cast-iron wall was identified, signifying that the cast-iron wall became essentially pinned at the base. No structural strength reduction was observed as a result of the crack formation, confirming the assumption that the out-of-plane strength of the cast-iron wall was insignificant to the X-direction response. Spalling in epoxy mortar repaired plastic hinges was minimal, and generally occurred at later drifts for the Repaired structure compared to the Original structure. Examples of the reduced level of spalling in the Repaired structure compared to the Original structure can be seen in Figure 8A–C for columns and beams. Limited spalling that did occur in the repaired hinges tended to concentrate in the original material directly adjacent to the repaired zone as can be seen in Figure 8A and B. Similar spalling performance has been observed in epoxy mortar repaired members in previous research.[17] It is thought that the lower stiffness of the epoxy mortar (~19% that of the original concrete; Table 3) in combination with its high strength allowed large compression strains to be induced in the repaired regions without extensive spalling. On the other hand, repaired zones where standard concrete was utilized (i.e., CW1 walls), spalling damage was similar for both the Original and Repaired structures (Figure 8D). Spalling in the CW1 walls did not extend beyond the assumed plastic hinge length, suggesting that the welded splice longitudinal reinforcement repair technique was effective.

10969845, 0, Downloaded from https://onlinelibrary.wiley.com/doi/10.1002/eqe.3818 by Tokyo Institute Of Technology, Wiley Online Library on [16/01/2023]. See the Terms and Conditions (https://onlinelibrary.wiley.com/terms-and-conditions) on Wiley Online Library for rules of use; OA articles are governed by the applicable Creative Commons License

TABLE 5 Input excitation sequence and damage characteristics of the Original and Repaired structures in the X-direction

	Original			Repaired			
Run	Magnitude	Δ_{max}, % [story]	V_{max}, kN	Magnitude	Δ_{max}, % [story]	V_{max}, kN	Salient damage characteristics
1	20%	0.07 [2]	51.2	20%	0.10 [2]	50.6	Initial cracking of structural members.
2	80%	0.31 [2]	167.0	80%	0.50 [3]	169.8	Increased cracking in members.
3	160%	0.65 [2]	292.4	120%	0.74 [3]	251.4	Wall edge longitudinal reinforcement yielding at base
3-2	-	-	-	180%	0.99 [4]	360.0	Beam longitudinal reinforcement yields in all stories. Wall centerline longitudinal reinforcement yields. Yielding of column longitudinal reinforcement at base and at the 4th story.
4	240%	1.36 [3]	402.9	240%	1.50 [4]	462.0	Beam-sway mechanism formed. Cracking at base of cast-iron wall.
5	260%	2.92 [2]	437.8	260%	2.13 [2]	494.7	Slight concrete cover spalling of CW1 wall end regions.
6	130%	2.20 [3]	290.1	220%	2.20 [2]	451.8	No detailed damage observation conducted.
7	220%	3.51 [2]	406.7	280%	3.00 [3]	514.3	First floor CW1 wall longitudinal reinforcement becomes visible.
8	220%	3.99 [2]	427.8	300%	4.19 [2]	518.0	Peak strength reached.
9	260%	5.60 [2]	444.2	300%	5.88 [2]	486.1	Spalling of concrete at several G1 beam ends Minor spalling above patched region of column X3-Y1 Crushing of end region core concrete and buckling of longitudinal reinforcement of CW1 walls.

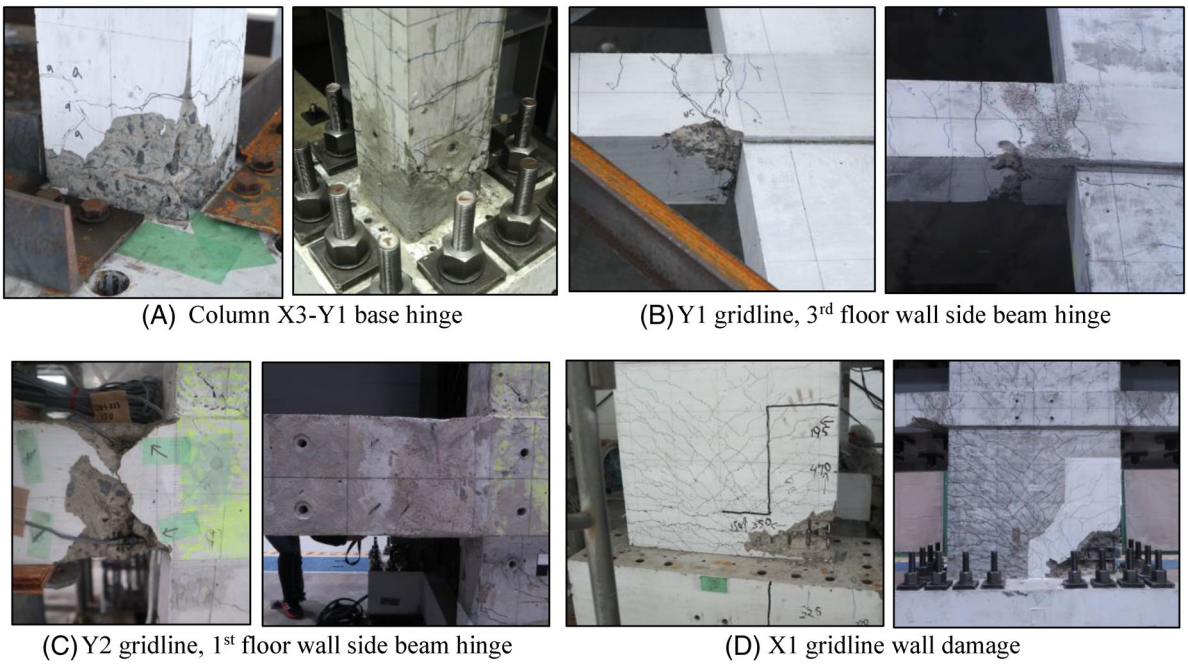

FIGURE 8 Comparison of damage pattern to beams, columns and walls at the conclusion of the Original (left) and Repaired (right) structure tests

10969845, 0, Downloaded from https://onlinelibrary.wiley.com/doi/10.1002/eqe.3818 by Tokyo Institute Of Technology, Wiley Online Library on [16/01/2023]. See the Terms and Conditions (https://onlinelibrary.wiley.com/terms-and-conditions) on Wiley Online Library for rules of use; OA articles are governed by the applicable Creative Commons License

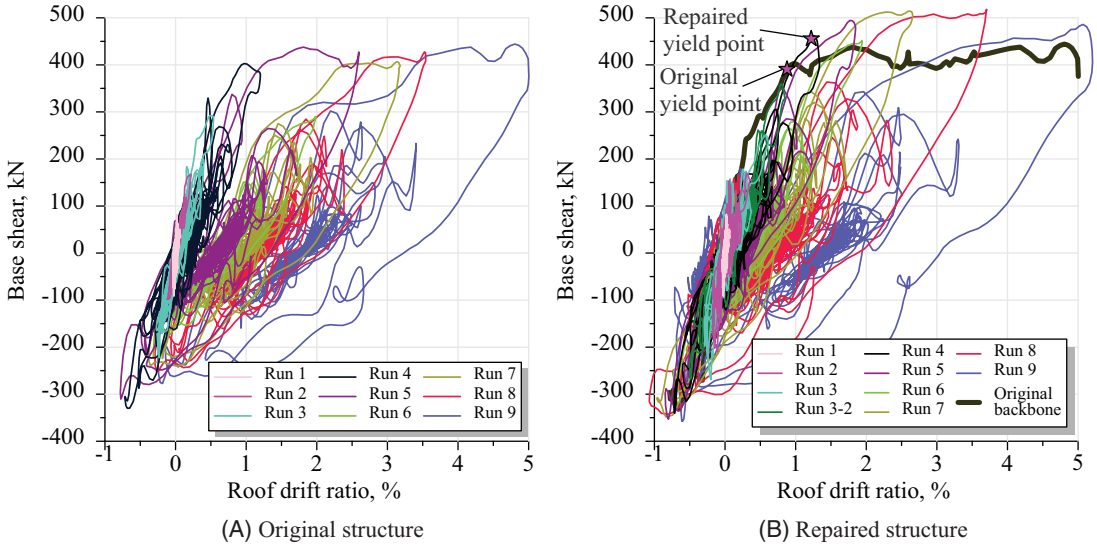

FIGURE 9 Base shear-roof drift ratio response of the (A) Original structure and (B) Repaired structure

6.3 | Force-displacement relationship and inter-story drift ratio distribution

The base shear-roof drift ratio relationship for the Original and Repaired structures are shown in Figure 9A and B, respectively. The envelope of the Original structure is traced as a grey line in Figure 9B for ease of comparison. Roof drift ratio was calculated as the cumulative sum of the inter-story drifts from each floor divided by the total height of the structure. The "yield points" of the Original and Repaired structures are also plotted in Figure 9B. The "yield point" corresponds to the formation of a full beam-sway mechanism in the structure. The full beam-sway mechanism was judged to have formed when strain in longitudinal reinforcement in all measured flexural hinges (beams, columns, and walls) exceeded the yield strain. From the comparison of Figure 9A and B the following observations can be readily made: (1) the stiffness of the Repaired structure leading up to the yield point is lower than that of the Original structure, (2) the apparent yield point of the Repaired structure has shifted to the right of the Original structure's yield point, (3) the hysteresis loops in the Repaired structure do not exhibit any obvious increase in pinching characteristics compared to the Original structure (i.e., no significant reinforcement bond degradation, or shear sliding along cracks), and (4) the strength of the Repaired structure is considerably higher than that of the Original structure. These aspects will be discussed in detail in the next section.

Maximum inter-story drift ratio distributions of the Original and Repaired structures are compared in Figure 10. Runs included in the comparison are those that achieve similar maximum roof drift ratios in both experimental programs (hereinafter "comparable Runs"). The purpose of this comparison is to make qualitative judgment on the shape of the drift ratio distribution rather than compare absolute magnitude. The maximum inter-story drift ratio distribution shape is very similar between the Original and Repaired structures suggesting no significant changes in the mode of vibration. Some minor difference is observed in the Repaired structure where the top inter-story drift ratio is slightly higher relative to the lower floors, when compared to the Original structure. This difference suggests that in the Repaired structure, upper stories are softer relative to the lower stories compared to the Original structure. Higher stiffness recovery in the lower floors is expected because of the higher intensity repair implemented (replacement of reinforcement and concrete) compared to the upper floors (epoxy injection only). Additionally, concrete cracks in the upper stories were generally narrower compared to that of the lower stories (particularly for columns and walls), resulting in likely reduced epoxy resin penetration depth.

7 | PERFORMANCE RECOVERY OF REPAIRED STRUCTURE

The primary objective of this study was to understand the effectiveness of basic repair techniques on the recovery of seismic performance of a damaged RC structure. Performance recovery is addressed from the perspective of stiffness, damping, deformation capacity, and strength. These four aspects will be systemically addressed in this section.

10969845, 0, Downloaded from https://onlinelibrary.wiley.com/doi/10.1002/eqe.3818 by Tokyo Institute Of Technology, Wiley Online Library on [16/01/2023]. See the Terms and Conditions (https://onlinelibrary.wiley.com/terms-and-conditions) on Wiley Online Library for rules of use; OA articles are governed by the applicable Creative Commons License

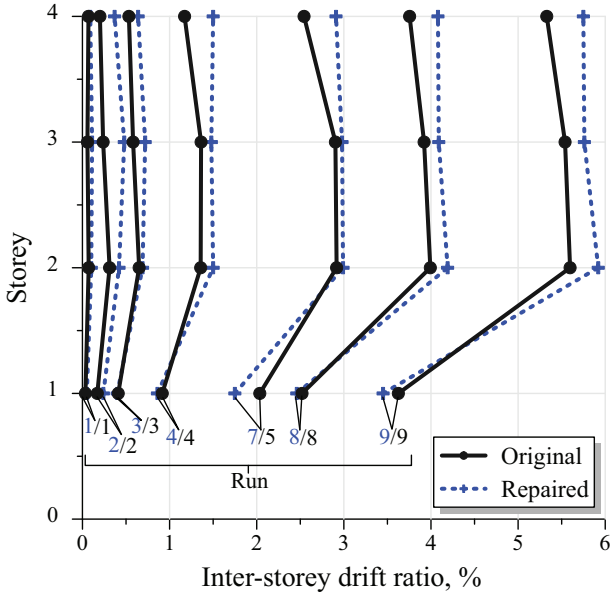

FIGURE 10 Maximum inter-story drift ratio distribution for runs resulting in similar peak roof drift ratio

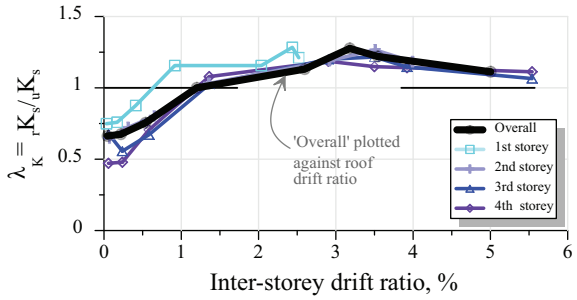

FIGURE 11 Recovery of secant stiffness, λ_K, for overall structure and for each storey

7.1 | Recovery of stiffness

The recovery of structural stiffness is an important consideration in estimating potential future force and deformation demands on the structure. In this section, secant stiffness recovery is investigated over several excitations of the Repaired structure. As the response hysteresis loops are rounded due to inherent damping, in this paper secant stiffness of each Run is calculated as the average of the secant stiffness to maximum base shear and the secant stiffness to maximum deformation of that Run. Yield secant stiffness is calculated using the yield points in Figure 9B. The recovery factor, λ_K, of the secant stiffness of the Repaired structure, ${}_rK_s$, to that of the Original structure, ${}_uK_s$ (where secant stiffness is calculated from the origin of the respective Run 1), is shown in Figure 11 for each comparable Run. The recovery factor is shown for both the "overall" response (i.e., using roof drift ratio) as well as that for each individual story, where accelerometer and inter-story drift data was used to get individual story stiffnesses. The "overall" initial stiffness of the Repaired structure (i.e., secant stiffness of Run 1) recovered to 66% of the Original structure. This number is similar to the 75% recovery ratio estimated from ambient vibration measurements, with the difference being due to the nature of the secant stiffness averaging method described above. These results show that despite a systematic and relatively extensive epoxy injection procedure the initial stiffness could not be fully recovered. This is likely due to a substantial number of cracks being too narrow or simply imperceptible to be effectively injected. Leading up to Run 4, secant stiffness recovery tends to be higher in the bottom stories (e.g., $\lambda_K = 0.75$ at first story for Run 1) compared to the top stories ($\lambda_K = 0.47$ at top story for Run 1). This tendency is consistent with the data in Figure 10 where lower stories exhibited relatively lower peak inter-story

10969845, 0, Downloaded from https://onlinelibrary.wiley.com/doi/10.1002/eqe.3818 by Tokyo Institute Of Technology, Wiley Online Library on [16/01/2023]. See the Terms and Conditions (https://onlinelibrary.wiley.com/terms-and-conditions) on Wiley Online Library for rules of use; OA articles are governed by the applicable Creative Commons License

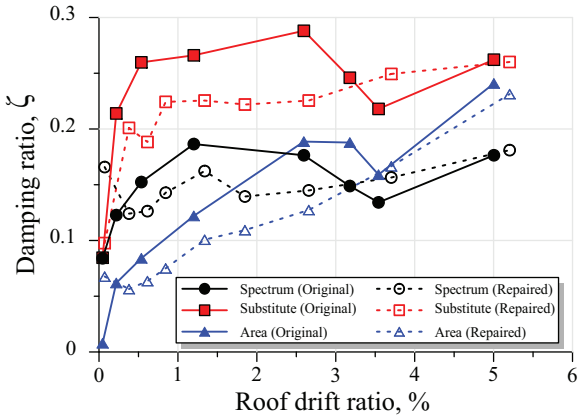

FIGURE 12 Equivalent viscous damping ratio of the Original and Repaired structures evaluated using three methods

drifts, and again suggests that the repair was more effective in the lower stories. Following Run 4, the Repaired structure exceeded the strength of the Original structure, resulting in secant stiffness higher than unity thereafter.

From Figure 9B, the yield point has shifted from 0.97% in the Original structure to 1.3% in the Repaired structure. This shift is not thought to be due to a reduction in post-cracking stiffness (e.g., due to Bauschinger effect) because the Run 4 hysteretic curve of the Repaired structure passes directly through the Original structure's yield point, as can be seen in Figure 9B. Rather, this shift is thought to be due to member sections developing higher yield curvatures due to higher section yield strengths.[29] This observation suggests that the overall structural strength increase seen in Figure 9 is due to inherent strength increase of individual members rather than a change in modal vibration characteristics. Based on the yield point definition in Figure 9B, the "overall" yield secant stiffness of the Repaired structure recovered to 87% of the Original structure.

7.2 | Recovery of equivalent viscous damping

Damping is necessary in structures to dissipate the input energy from earthquakes; therefore, it is critical to understand how much damping capacity can be recovered through structural repairs. Three calculation methods were used to evaluate the equivalent viscous damping ratio, ζ_{eq}, for each comparable Run. The "spectrum" method utilized the capacity spectrum approach, where for each Run the design demand spectrum in Figure 3 (scaled to the respective Run magnitude in Table 5) was adjusted by a damping reduction factor, F_h, in Equation (4), until an intersection with the capacity curve of the structure was obtained.[30] The corresponding damping ratio, $\zeta_{spectrum}$, was then back calculated from F_h using Equation (4).[19] As Equation (4) is an empirical formula, the "spectrum" method will naturally yield empirical estimates of damping ratio. In the "substitute" method all energy dissipated during the entire dynamic response history is assumed to be due to viscous damping. Using an equivalent single degree of freedom response of the structure, the substitute damping ratio, $\zeta_{substitute}$, can then be calculated using Equations (5–6).[31] This method assumes that all of the energy input into the structure is dissipated through viscous damping, and thus provides a single "average" damping value over the duration of the excitation. Finally, in the "area" method the equivalent viscous damping ratio, ζ_{area}, is calculated using Equations (7–8), where the ΔW is taken as the area inside the largest half-cycle hysteresis loop of each Run and W_e is the strain energy corresponding to the maximum deformation of that cycle.[32] In this calculation method it is assumed that the structure is under resonant, steady-state response, though this is not the case in random vibration. The damping ratio calculated via each method and for each comparable Run of the Original and Repaired structures is plotted against the maximum roof drift ratio of the corresponding Run in Figure 12.

$$F_h = \frac{1.5}{1 + 10\zeta_{spectrum}} \tag{4}$$

$$\zeta_{\text{substitute}} = -\frac{\int_0^t \ddot{u}_{0g}\dot{u}dt}{2\omega_e \int_0^t \dot{u}^2 dt} \tag{5}$$

10969845, 0, Downloaded from https://onlinelibrary.wiley.com/doi/10.1002/eqe.3818 by Tokyo Institute Of Technology, Wiley Online Library on [16/01/2023]. See the Terms and Conditions (https://onlinelibrary.wiley.com/terms-and-conditions) on Wiley Online Library for rules of use; OA articles are governed by the applicable Creative Commons License

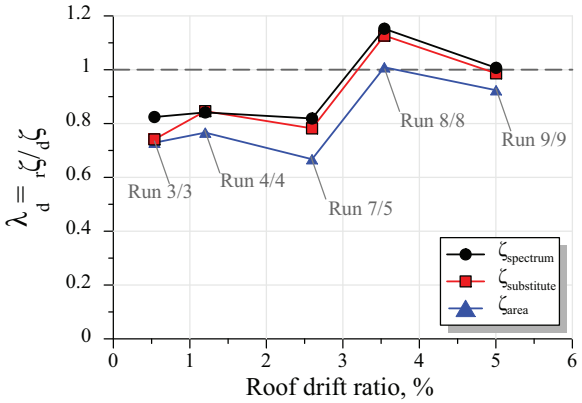

FIGURE 13 Recovery of damping ratio for each Run (Original/Repaired)

$$\omega_e = \sqrt{(S_{a,max} - S_{a,min})/(S_{d,max} - S_{d,min})} \tag{6}$$

$$\zeta_{\text{area}} = \frac{1}{4\pi} \frac{2\Delta W}{W_e} \tag{7}$$

$$W_{\text{e}} = \frac{1}{2} \frac{V_{u_{max}}}{u_{max}} \tag{8}$$

where F_h is the design spectrum reduction factor due to damping, $\ddot{u}_{0g}$ is the input acceleration time history measured at the structure's foundation level, $\dot{u}$ is the first mode velocity response of the structure, t is the total duration of the excitation, ω_e is the equivalent structural natural cyclic frequency corresponding to each Run, $S_{d,max}$ and $S_{d,min}$ are the maximum and minimum spectral displacement values for each Run, respectively and $S_{a,max}$ and $S_{a,min}$ are the corresponding spectral acceleration values. u_{max} and $V_{u_{max}}$ are the maximum roof drift and the corresponding base shear, respectively.

From Figure 12 it can be seen that the absolute value of the equivalent viscous damping ratio varies significantly between each calculation method. The level of variability tends to decrease with increasing roof drift ratio of the structure. The "substitute" method results in the highest damping ratios (above 20% for both Original and Repaired structures). The "spectrum" method produces higher damping ratios than the "area" method up until roof drifts of around 3%, after which the trend is reversed, such that the "area" method produces higher damping ratios. The large variability in the damping ratio between methods is not unexpected given the fundamentally different theoretical and empirical assumptions in the calculations. These differences have been previously shown to have a dependence on the structural period, ductility and hysteresis shape.[33] In this study, the focus is given on the level of recovery of damping ratio rather than the absolute magnitudes. To calculate the damping capacity recovery factor, λ_d, the damping ratios for the Repaired structure were normalized by that of the Original structure for comparable Runs. The results are shown in Figure 13 (Run 1 and 2 data are excluded as large scatter was obtained when executing the quotient operation in the elastic region of the response). The comparison shows that despite large differences in the absolute damping ratio values seen in Figure 12, the magnitude of the damping recovery factor is generally in agreement between all three calculation methods for the Runs shown. The damping capacity recovery factor is approximately $\lambda_d \approx 80\%$ up to 2.7% roof drift (i.e., Run 7/5 in Figure 13). This suggests that the damping capacity is only partially recovered at low-moderate seismic demands. The loss of damping capacity is attributed to imperfect restoration of the concrete performance (e.g., deficiencies in epoxy injection technique to reseal all cracks). On the other hand, at higher drifts (Run 8/8 and Run 9/9) corresponding to higher levels of damage, the damping capacity recovery factor is close to or slightly exceeding 1.0. At these high drift demands, concrete is generally fully cracked and so energy dissipation capacity is largely governed by the plastic deformation of reinforcement; thus, reduction in damping capacity is not expected provided there is no degradation in performance of reinforcement. Given these results, in simplified models of repaired structures that utilize some form of equivalent linearization of the beam-sway structural system, using a lower bound damping capacity recovery factor of 80% may be appropriate.

10969845, 0, Downloaded from https://onlinelibrary.wiley.com/doi/10.1002/eqe.3818 by Tokyo Institute Of Technology, Wiley Online Library on [16/01/2023]. See the Terms and Conditions (https://onlinelibrary.wiley.com/terms-and-conditions) on Wiley Online Library for rules of use; OA articles are governed by the applicable Creative Commons License

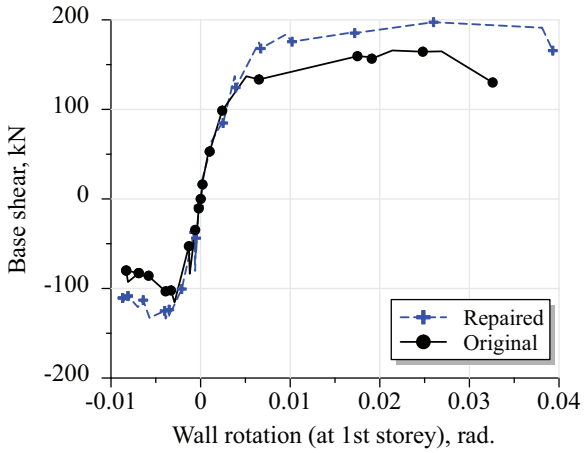

FIGURE 14 Plastic h inge rotation-base shear curve of the instrumented CW1 wall (Run 6 not shown)

7.3 | Recovery of deformation capacity

Structural members in beam-sway structures must possess adequate deformation capacity to ensure sufficient earthquake energy absorption can occur. Structural members experiencing reduced deformation capacity due to repairs may no longer possess the necessary ductility to justify the shear force reduction factors assumed in the design. While neither the Original nor the Repaired structures were allowed to reach a level of total collapse during the experiments (due to safety concerns), some inferences can be made on deformation capacity based on the available data. The only X-direction members to have experienced failure in both testing programs were the CW1 walls (Figure 8D). The measured wall rotation-base shear backbones of the CW1 wall response in the Original and Repaired structures are shown in Figure 14. It can be observed from Figure 14 that both the Original and Repaired walls experienced significant strength degradation in the final run, which coincided with observation of concrete crushing and longitudinal reinforcement buckling in the corners of the wall (Figure 8D). The maximum rotation of the CW1 wall in the Repaired structure prior to the significant strength degradation (0.038 rad.) exceeded that of the Original structure wall (0.027 rad.), suggesting that deformation capacity was fully recovered. Higher deformation capacity of the CW1 walls in the Repaired structure is thought to be due to the replacement concrete being slightly softer than the original material (Table 3) combined with the softening of the beams that frame into the wall, allowing higher section curvatures to be attained in the wall. This data suggests a deformation capacity recovery factor $\lambda_{dc} = 1.0$ is appropriate for flexural walls, which is also in agreement with the value in the FEMA 306 guidelines. From the perspective of system-level performance, though the maximum deformation capacity at collapse is unknown, it can be seen in Figure 10 that inter-story drift ratio exceeded 5% in both structures. This is generally outside the typical range of drift demands expected on buildings, so it can be said that for a practical range of drift demands, deformation capacity was fully recovered following repairs.

7.4 | Recovery of strength

An unexpected increase in structural strength due to repair can be detrimental to structural performance if it disrupts the intended hierarchy of strength between and within individual structural members. For example, an increase in flexural strength of a member above its shear strength can cause a transition of failure mechanism from a ductile flexural failure to brittle shear failure. As can be seen in Figure 9, the strength of the Repaired structure increased compared to the Original structure. Specifically, an increase of 17% ($\lambda_s = 1.17$) was observed for both yield and maximum strength. The strength increase is thought to be due to either (1) a change in mode shape of the response, (2) effect of strengthening of the structure's Y-direction, (3) strain hardening of reinforcement, or (4) strain aging of reinforcement.

Similarity in the maximum deformation profiles shown in Figure 10 suggests that the strength increase was unlikely due to changes in the vibration mode shape. The effect of the cast-iron block wall installed in the Y-direction is also not thought to be significant due to the early development of a crack under weak-direction loading at the base of the wall.

10969845, 0, Downloaded from https://onlinelibrary.wiley.com/doi/10.1002/eqe.3818 by Tokyo Institute Of Technology, Wiley Online Library on [16/01/2023]. See the Terms and Conditions (https://onlinelibrary.wiley.com/terms-and-conditions) on Wiley Online Library for rules of use; OA articles are governed by the applicable Creative Commons License

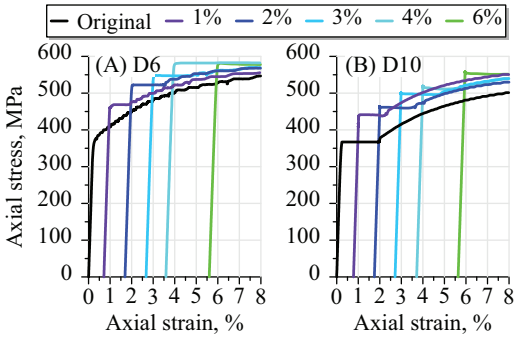

FIGURE 15 Stress-strain relationship of D6 and D10 reinforcement before and after strain aging

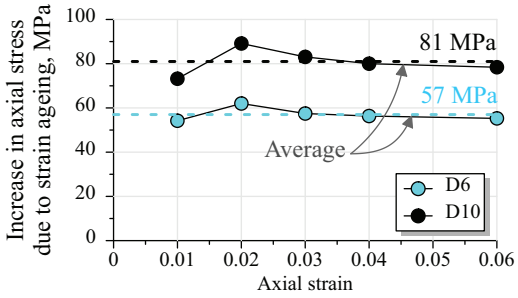

FIGURE 16 Increase in strength attributed to strain aging for D6 and D10 reinforcement

Therefore, a combination of reinforcement strain hardening and strain aging are thought to be the principal causes for the observed strength increase. The presence of strain aging also helps explain the absence of Bauschinger effect in Figure 9, as previous studies have demonstrated that the Bauschinger effect is "reset" by strain aging.[35] Previous studies on strain aged reinforcement have indicated that a strength increase of 10%–20% of the original yield stress can be expected, and that this value is somewhat independent of the maximum previously exerted strain.[34–37] To confirm whether strain aging was a cause of the observed strength increase in the present study, longitudinal reinforcement used in the beams (D6 bars), columns and walls (D10 bars) were tested. The test procedure involved subjecting the reinforcement to an initial tensile strain ranging from 1%–6% (strain ranges recorded in members of the Original structure); unloading and allowing the bars to age; and finally reloading the bars until tensile fracture. The aging process was accelerated by heat treating the bars at 100°C for 4 h, to simulated 1-year of strain aging[38] (the period between testing of the Original and Repaired structures). The stress-strain curves for the "original" non-aged reinforcement and strain-aged reinforcement are shown in Figure 15. It can be seen that after the strain aging process the yield stress of both the D6 and D10 reinforcement exceeded the envelope of the "original" reinforcement. The strain aged reinforcement curves also exhibit reemergence of the yield-plateau, which would otherwise not be present had reloading occurred immediately after unloading from the initial strain. This provides evidence for the disappearance of the Bauschinger effect and an explanation of why the backbone of the Repaired structure in Figure 9B passes through the yield point of the Original structure. The increase in stress directly attributed to strain aging (i.e., excluding the effect of strain hardening) for each bar diameter is shown in Figure 16. It can be seen that while the magnitude of the stress increase is different for the D6 and D10 reinforcement, it is essentially independent of the initially applied peak strain level, provided yielding has occurred. On average, the increase in stress is 57 MPa for D6 reinforcement and 81 MPa for D10 reinforcement. Expressed as a percentage relative to the expected stress at the corresponding strain level for a non-aged bar, this becomes 12% and 19% for D6 and D10 reinforcement, respectively.

To confirm if the increase in reinforcement strength is consistent with the overall 17% structural strength increase measured experimentally, a comparison was made between the sum of the moment capacity, $M_{u,total}$, of all plastic hinges in the Repaired and Original structures (i.e., 4 C1 column hinges, 32 G1 beam hinges and 2 CW1 wall hinges). The individual hinge strengths, M_u, were calculated using the Architectural Institute of Japan standard[21] (with exception of CW1,

10969845, 0, Downloaded from https://onlinelibrary.wiley.com/doi/10.1002/eqe.3818 by Tokyo Institute Of Technology, Wiley Online Library on [16/01/2023]. See the Terms and Conditions (https://onlinelibrary.wiley.com/terms-and-conditions) on Wiley Online Library for rules of use; OA articles are governed by the applicable Creative Commons License

TABLE 6 Estimated increase in total structural strength capacity due to strain aging

	Original		Repaired	
	M_u kNm	$M_{u,total}$, kNm	M_u, kNm	$M_{u,total}$, kNm
C1	7.0	28.0	8.0	32.0
G1 (+ve)[a]	4.4	70.4	4.9	78.4
G1 (−ve)	10.0	160.0	10.5	168.0
CW1	246.0	492.0	287.4	574.8
Total capacity		**750.4**		**853.2**

[a] +ve refers to positive bending, that is, top fiber in compression, and −ve refers to negative bending, that is, top fiber in tension.

where moment capacity was calculated from section analysis as the point at which the extreme concrete compression fiber reached a strain 0.003). To account for strain aging in the calculations, the yield stress of longitudinal reinforcement was increased from the original strengths in Table 4 by the average values indicated in Figure 16. The total capacity results for the Original and Repaired structures are listed in Table 6. From this rough calculation a 13.7% overall increase in structural strength is estimated in the Repaired structure, which is only slightly lower than the experimentally determined 17%. The results of this sub-study suggest that strain aging was the principal cause of the observed 17% increase in strength of the Repaired structure. Though strain hardening was not directly quantified (due to uncertainty of the strain state of reinforcement following correction of the Original structure's residual drift), the above results suggest that it had a relatively minor contribution to the increase in overall strength. As a strength increase of this magnitude can lead to potentially unexpected failure modes, it follows that strain aging should be an important consideration in the repair decisions of damaged structures. It is acknowledged that the range of parameters considered in this material sub-study is limited; a detailed investigation on other commonly used steel grades as well as realistic strain histories (cyclic loading) should be undertaken in the future.

8 | CONCLUSIONS

The objective of this study was to quantify the degree of structural performance recovery achieved from the repair of RC structures exhibiting flexural damage characteristics. Specifically, the focus was on utilizing relatively simple and common repair techniques, as opposed to "strengthening" interventions. As part of the investigation, a previously tested ¼ scale 4-storey RC structure was repaired and retested on a shake table. From damage observations and from the measured structural response data, the following conclusions are made on the structural performance recovery:

1. Damage characteristics: The degree of visually observed damage in the Repaired structure was generally less severe (i.e., less spalling) compared to that in the Original structure. This difference is largely attributed to the low stiffness and high strength of the epoxy mortar used in the repair of previously spalled areas.
2. Stiffness (initial): Period measurements during the repair process indicated that epoxy injection of the beams and slabs resulted in the highest effect on initial stiffness recovery. Experimental data shows that despite an extensive crack epoxy injection procedure, overall initial stiffness recovered to only 66% of the Original structure (stiffness recovery factor tended to be higher in the lower stories of the structure where concrete replacement repair was undertaken). It is thought that full stiffness recovery could not be achieved due to a substantial number of cracks being too narrow to be effectively injected.
3. Stiffness (secant yield): The yield point of the Repaired structure shifted to 1.3% roof drift ratio from 0.97% in the Original structure. The shift in yield point is thought to be due to the increase in structural strength (i.e., not Bauschinger effect) because the Repaired backbone passed through the yield point of the Original structure. The corresponding yield secant stiffness recovery was 87%.
4. Equivalent viscous damping: The magnitude of calculated damping ratio varied significantly depending on the method of calculation used. However, when examined as a ratio of Repaired to Original performance, the recovery of damping capacity was in agreement between all methods. An average damping capacity recovery factor was 80% in low-moderate drifts, thought to be due to the incomplete effectiveness of crack epoxy injection. At high drifts, where energy dissipation is governed by reinforcement yielding, 100% recovery was achieved.

10969845, 0, Downloaded from https://onlinelibrary.wiley.com/doi/10.1002/eqe.3818 by Tokyo Institute Of Technology, Wiley Online Library on [16/01/2023]. See the Terms and Conditions (https://onlinelibrary.wiley.com/terms-and-conditions) on Wiley Online Library for rules of use; OA articles are governed by the applicable Creative Commons License

5. Deformation capacity: Both the Original structure and the Repaired structure exceeded 5% inter-story drift ratio. Given that this is higher than the typically expected drift demands in structures, it can be said that practically full recovery of deformation capacity was achieved. Furthermore, the plastic hinge rotation at failure of the X-direction walls was essentially identical between the two structures, indicating the wall deformation capacity was fully recovered.
6. Strength: Yield strength and maximum strength of the Repaired structure increased by 17% compared to the Original structure. A material sub-study confirmed that the reinforcement used in the structure was susceptible to increase in strength due to strain aging effects. The magnitude of the stress increase was in the range of 12%–19% of peak stress from initial loading, depending on the type of reinforcement. These results suggest that strain aging was the principal cause of the overall structural strength increase.

ACKNOWLEDGMENTS

The research presented in this paper was jointly funded by Obayashi Corporation and the Consortium for Socio-functional Continuity Technology (http://www.softech.titech.ac.jp/; Project ID: JPMJOP1723 under Japan Science and Technology Agency). The authors would also like to express their gratitude to the University of Auckland's Professor Kenneth Elwood and Dr. Lucas Hogan for the advice received during the repair stages of the project. Lastly, thanks are extended to the group of technical staff at Obayashi Corporation and members of Maeda Lab who helped execute the experiment and perform damage observations on the structure.

DATA AVAILABILITY STATEMENT

The data that support the findings of this study are available from the corresponding author upon reasonable request.

ORCID

Alex V. Shegay https://orcid.org/0000-0002-4678-7000
Kota Miura https://orcid.org/0000-0002-7832-1977
Masaki Maeda https://orcid.org/0000-0002-4223-0766

REFERENCES

1. United Nations. *Transforming our world: The 2030 Agenda for Sustainable Development A/RES/70/1. Available from*; 2015. https://sdgs.un.org/sites/default/files/publications/21252030%20Agenda%20for%20Sustainable%20Development%20web.pdf
2. Marquis F, Kim JJ, Elwood KJ, Chang SE. Understanding post-earthquake decisions on multi-storey concrete buildings in Christchurch, New Zealand. *Bull Earthq Eng.* 2017;15(2):731–758. https://doi.org/10.1007/s10518-015-9772-8
3. FEMA 306. *Evaluation of Earthquake Damaged Concrete and Masonry mWall Buildings: Basic Procedures Manual*. Redwood City, CA: 1998.
4. FEMA 308. *Repair of Earthquake Damaged Concrete and Masonry Wall Buildings*. Redwood City, CA: 1998.
5. Federal Emergency Management Agency. *NEHRP Guidelines for the Seismic Rehabilitation of Buildings (FEMA 273)*.Redwood City, CA: 1997.
6. American Society of Civil Engineers/Structural Engineering Institute (ASCE/SEI). Seismic Evaluation and Retrofit of Existing Buildings. ASCE/SEI 41-17. Renton, VA; 2017. https://doi.org/10.1061/9780784414859
7. Japan Building Disaster Prevention Association. Guidelines for Post-earthquake Damage Evaluation and Rehabilitation of RC Buildings (in Japanese). Tokyo, Japan; 2015.
8. Celebi M, Penzien J. *Hysteretic Behavior of Epoxy Repaired RC Beams*. Birkeley, California. Report No. EERC 73/05, Earthquake Engineering Research Center, Berkley, CA: 1973. https://nisee.berkeley.edu/elibrary/eerc/1973
9. Lee DLN, Wight JK, Hanson RD. *Original and Repaired Reinforced Concrete Beam-Column Subassemblages Subjected to Earthquake Type Loading*. UMEE Report 76S4. Ann Arbor, MI; 1976.
10. Cuevas A, Pampanin S. Post-seismic capacity of damaged and repaired reinforced concrete plastic hinges extracted from a real building. Proceedings of the 2017 New Zealand Society for Earthquake Engineering Conference, Paper No. 3142; 2017.
11. Marder KJ, Elwood KJ, Motter CJ, Charles Clifton G. Quantifying the effects of epoxy repair of reinforced concrete plastic hinges. *Bull NZ Soc Earthq Eng.* 2020;53(1):37–51. https://doi.org/10.5459/BNZSEE.53.1.37-51
12. Lehman DE, Gookin SE, Nacamull AM, Moehle JP. Repair of earthquake-damaged bridge columns. *ACI Struct J.* 2001;98(2):233–242. https://doi.org/10.14359/10192
13. Tasai A. Resistance of flexural reinforced concrete members after repair with epoxy resin. Ninth World Conference on Earthquake Engineering, No. 12-3-2. August 2-9. Tokyo-Kyoto, Japan; 1988.
14. Motter CJ, Clauson AB, Petch JC, Hube MA, Henry RS, Elwood KJ. Seismic performance of repaired lightly reinforced concrete walls. *Bull N Z Soc Earthq Eng.* 2017;50(4):574–585.
15. Iliya R, Bertero V V. Effects of amount and arrangement of wall-panel reinforcement on hysteretic behavior of reinforced concrete walls. Report No. EERC 80/04; 1980.

10969845, 0, Downloaded from https://onlinelibrary.wiley.com/doi/10.1002/eqe.3818 by Tokyo Institute Of Technology, Wiley Online Library on [16/01/2023]. See the Terms and Conditions (https://onlinelibrary.wiley.com/terms-and-conditions) on Wiley Online Library for rules of use; OA articles are governed by the applicable Creative Commons License

16. Wang TY, Bertero VV, Popov EP. *Hysteretic behavior of reinforced concrete framed walls. Report No. EERC 75/23, Earthquake Engineering Research Center*, Berkeley, CA: 1975. https://nisee.berkeley.edu/elibrary/eerc/1975
17. Wight JK, Jirsa JO, Corley WG. *SP-084: Earthquake effects on reinforced concrete structures – US Japan research. ACI Symposium Publication 84*; 1984. https://doi.org/10.14359/14041
18. Miura K, Fujita K, Tabata Y, Maeda M, Shegay A, Yonezawa K. Shake-table test of a 4-storey frame-wall RC strcture to investigate the collapse mechanism and safety limit (in Japanese). *J Struct Constr Eng.* 2021;86(780):247–257.
19. Building Center of Japan. The *Building Standard Law of Japan* . Building Center of Japan. Tokyo, Japan; 2016. ISBN 978-4-88910169-0.
20. Architectural Institute of Japan. *Design Guidelines for Earthquake Resistant Reinforced Concrete Buildings Based on Inelastic Displacement Concept*. Architectural Institute of Japan. Tokyo, Japan: 1999.
21. Architectural Institute of Japan. *AIJ Standard for Structural Calculation of Reinforced Concrete Structures (in Japanese)*. Architectural Institute of Japan. Tokyo, Japan: 2018.
22. Standards New Zealand. NZS 3101:2006: Concrete Structures Standard Part 1 - The Design of Concrete Structures (Amendment 3). Wellington, New Zealand; 2017.
23. American Concrete Institute. *Building Code (ACI 318–19) and Commentary on Building Code Requirements for Structural Concrete (ACI 318R-19)*; 2019.
24. British Standards Institution. EN 1998-1:2004/A3:2013: Eurocode 8: Design of structures for earthquake resistance. Part 1: General rules, seismic actions and rules for buildings. London, United Kingdom; 2013. https://doi.org/10.3403/03244372
25. Anabuki T, Masuda Y, Kurita K, et al. Shake-table test of a 4-story repaired and retrofitted RC structure to evaluate seismic capacity. Part 4: Behavior of seismic walls in the Y-direction (in Japanese). AIJ Annual Conference Proceedings, Architectural Institute of Japan. Paper No. 23235. Tokyo Japan; 2021: 469-470.
26. Maeda M, Al-Washali H, Matsukawa K. An overview of post earthquake damage and residual capacity evaluation for reinforced concrete buildings in Japan. 7th International Conference on Computational Methods in Structural Dynamics and Earthquake Engineering Methods in Structural Dynamics and Earthquake Engineering; 2019:930–943. https://doi.org/10.7712/120119.6969.19228
27. Building Maintenance and Management Center. *Building Repair Work Supervision Guideline (in Japanese)*. Building Maintenance and Management Center, Tokyo Japan; 2019.
28. Anabuki T, Kobayashi M, Hagio H, Miura K, Masuda Y. Development of the "3Q-Wall®" retrofitting method using casting blocks. *Obayashi Tech Res Rep.* 2017;(81):1–8.
29. Priestley MJN, Kowalsky JM. Aspects of drift and ductility capacity of rectangular cantilever structural walls. *Bull NZ Soc Earthq Eng.* 1998;31(2):73–85.
30. Freeman SA. The Capacity Spectrum Method for Determining the Demand Displacement. ACI 1994 Spring Convention, 1994: 1-7.
31. Gulkan P, Sozen M. Inelastic responses of reinforced concrete structures to earthquake motions. *Proc ACI.* 1974;71(12):604–610.
32. Jennings P. Equivalent viscous damping for yielding structures. *J Eng Mech Div.* 1968;94(1):103–116. https://doi.org/10.1061/JMCEA3.0000929
33. Judi HJ, Fenwick RC, Davidson BJ. Direct displacement based design - a definition of damping. Proceedings of the 2001 New Zealand Society for Earthquake Engineering Conference. New Zealand Society for Earthquake Engineering, Christchurch, New Zealand; 2001.
34. Pussegoda LN. Strain age embrittlement in reinforcing steels. Ph.D Thesis. University of Canterbury; 1978.
35. Momtahan A, Dhakal RP, Rieder A. Effects of strain-ageing on New Zealand reinforcing steel bars. *Bull NZ Soc Earthq Eng.* 2009;42(3):179–186. https://doi.org/10.5459/bnzsee.42.3.179-186
36. Loporcaro G. *A least invasive method to estimate the residual strain capacity of steel reinforcement in earthquake-damaged buildings.* Ph.D Thesis. University of Canterbury; 2017.
37. Dodd LL, Restrepo-Posada JI. Model for predicting cyclic behavior of reinforcing steel. *J Struct Eng.* 1995;121(3):433–445. https://doi.org/10.1061/(asce)0733-9445(1995)121:3(433)
38. Hundy BB. Accelerated strain ageing of mild steel. *J Iron Steel Int.* 1954;(A):49–62.

How to cite this article: Shegay AV, Miura K, Akira M, Maeda M, Seki M. Performance recovery of a repaired 4-storey reinforced concrete structure subjected to shake-table testing. *Earthquake Engng Struct Dyn*. 2023;1-21. https://doi.org/10.1002/eqe.3818

APPENDIX A

The JBDPA Guidelines[7] provide performance recovery factors for repaired structural members. These are reproduced in Table A1. The exact method of implementation of these factors is not described in the JBDPA Guidelines, though it is assumed that the intention is similar to the FEMA 306[3] factors (i.e., to be used in hinge models of repaired members). The factors are not specific to a performance characteristic (i.e., strength, stiffness, deformation capacity). They are also given as a value range as opposed to deterministic values. These areas of ambiguity imply that considerable engineering judgment is expected to be exercised in implementing the performance recovery factors. The recovery factors vary depending on the type of member, the extent of repair work and the damage level (defined in[7]; Appendix B).

10969845, 0, Downloaded from https://onlinelibrary.wiley.com/doi/10.1002/eqe.3818 by Tokyo Institute Of Technology, Wiley Online Library on [16/01/2023]. See the Terms and Conditions (https://onlinelibrary.wiley.com/terms-and-conditions) on Wiley Online Library for rules of use; OA articles are governed by the applicable Creative Commons License

TABLE A1 Member performance recovery factors following repair and strengthening

Repair methodology				Damage Level II	III	IV	V
Individual repair	Column	C1	Repair of cracks	0.95–1.0	0.9–0.95		
		C2	Repair of spalled concrete		0.9–0.95	0.8–0.9	
		C3	Shear strengthening[a]: Welding, confinement wrapping, plate	0.95–1.0	0.9–0.95	0.8–0.9	0.8–0.9
	Wall	W1	Repair of cracks		0.9–0.95		
		W2	Repair of spalled concrete		0.9–0.95	0.8–0.9	
		W3	Shear strengthening[a]: Partial recasting, total recasting, section enlargement		0.9–0.95	0.8–0.9	0.7–0.8
Combined repair		C1 and C2		1.0	0.95–1.0		
		C1 and C3[a]			0.95–1.0	0.9–1.0	
		C1, C2 and C3[a]			0.95–1.0	0.9–1.0	0.8–0.9
		W1 and W2		1.0	0.95–1.0		
		W1 and W3[a]			0.95–1.0	0.9–1.0	
		W1, W2 and W3[a]			0.95–1.0	0.9–1.0	0.8–0.9

[a]If accurate calculations can demonstrate that strength will exceed the original member strength (pre-damage), a factor of more than 1.0 may be adopted.

APPENDIX B

The JBDPA Guidelines[7] provide a damage assessment methodology for individual reinforced concrete (RC) members

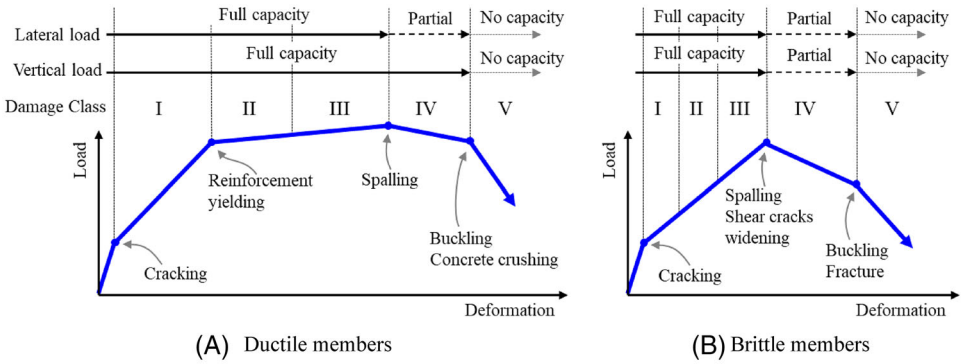

FIGURE B1 Visual representation of damage states for ductile and brittle members

based on visual observation. All damage is broadly classified into five damage levels, the definitions of which are summarized in Table B1. The damage levels can be shown to represent various parts of the member force-deformation backbone curve for ductile (flexural) and brittle (shear) members, as shown in Figure B1.

TABLE B1 Definition of damage levels of structural members

Damage level	Observed damage in structural members
I	Sparse, fine cracks can be observed (<0.2 mm). No reinforcement yielding expected.
II	Clearly visible cracks (0.2–1 mm) exist.
III	Wide cracks (1–2 mm) are present. Plastic hinging mechanisms begin to form. Some spalling of cover concrete is observed but concrete core is in-tact.
IV	Many wide cracks are observed. Compression damage resulting in concrete spalling and exposed reinforcement. Lateral strength degradation may occur, but vertical load is still fully carried by walls and columns.
V	Buckling (and in some cases fracture) of reinforcement, crushing of concrete and vertical deformation of columns and/or shear walls observed. Settlement and inclination of structure are characteristic.

10969845, 0, Downloaded from https://onlinelibrary.wiley.com/doi/10.1002/eqe.3818 by Tokyo Institute Of Technology, Wiley Online Library on [16/01/2023]. See the Terms and Conditions (https://onlinelibrary.wiley.com/terms-and-conditions) on Wiley Online Library for rules of use; OA articles are governed by the applicable Creative Commons License